Nuclear Inst. and Methods in Physics Research, A 1038 (2022) 166834

Contents lists available at ScienceDirect

Nuclear Inst. and Methods in Physics Research, A

journal homepage: www.elsevier.com/locate/nima

Design and optimisation of the Compact Linear Collider main LINAC module for micron-level stability and alignment

Matthew Capstick [a,*], Steffen Doebert [a], Markus Aicheler [a,b], Carlo Rossi [a]

[a] CERN, European Organisation for Nuclear Research, Geneva, Switzerland
[b] Helsinki Institute of Physics, Finland

ARTICLE INFO

Keywords:
Alignment
CLIC
Emittance preservation
FEA
Harmonic analysis
Luminosity
Modal analysis
Stability
TBM
Vibration

ABSTRACT

The Compact Linear Collider (CLIC) study is developing a Multi-TeV e^+e^- linear collider. An acceleration gradient of 100 MV m^{-1} will be achieved in the Main LINACs using 11.994 GHz Super Accelerating Structures (SAS). To achieve the required luminosity, the SAS will be prealigned within modules to less than 14 μm and maintain their position to within 1.4 μm when exposed to local sources of mechanical noise. A module design is presented and Finite Element Analysis (FEA) is used to optimise the harmonic frequencies of this module and thereby minimise the potential impact of unknown sources of vibration. A module with a fundamental frequency of 60 Hz is presented. Historical ground noise data from the LHC at CERN is used to statistically quantify the magnitude of SAS misalignments unavoidably induced by local ground noise. The one-standard-deviation average vertical misalignment due to ground noise is less than 0.044 μm above 0.1 Hz for all SAS.

1. Introduction

The Compact Linear Collider (CLIC) is a proposed electron–positron collider with a centre-of-mass collision energy up to 3 TeV [1] and a high luminosity of 1.5×10^{34} cm^{-2} s^{-1} [2]. CLIC is based on a novel two-beam acceleration scheme that utilises a low-energy high-intensity Drive Beam to supply the RF power to a high-energy Main Beam. To achieve the required luminosity an extremely low Main Beam normalised vertical emittance (20 nm) at the end of the LINAC is required [3]. The main source of emittance growth is the misalignment of the accelerator components which causes transverse deflections, introduces dispersions, and produces wakefields in the accelerator structures, therefore tight static and dynamic position tolerances for the Main Beam and Drive Beam components are required [3,4]. CLIC is designed to initially produce a collision energy of 380 GeV before later being expanded to a collision energy of 3 TeV. The r.m.s. jitter tolerances for the Accelerator Structures within the 3 TeV version of CLIC are given in Table 1. For the 380 GeV CLIC the same alignment tolerances will allow operation at a greater luminosity. After the initial prealignment the alignment of both the Main Beam and Drive Beam components will be maintained using a remotely controlled active alignment system [3]. Beyond this, a beam-based alignment system will be used to achieve the final alignment required. To simplify the integration and alignment, and to reduce the cost of the system, the individual Super Accelerating Structures will not be independently actuated, but several SAS will be mounted to a single common structure which will then be actively positioned. Finally, this assembly of several SAS is closely integrated with a similar section of the drive beam forming a Two Beam Module (TBM) that can be positioned to within the CLIC alignment specification, as shown in Fig. 1.

To prevent a luminosity loss of greater than 1%, the SAS position must be kept within the jitter tolerance provided in Table 1, even when exposed to unavoidable sources of vibration such natural ground noise and mechanical vibration from water cooling circuits or forced airflow [5]. One way in which the suitability of the module design is being evaluated is based on the frequency of the harmonic modes of the system. Previous experiments have demonstrated that large Accelerating Structure displacements can be produced by varying the flow conditions of the water cooling circuit and producing vibrations close to the natural frequency of the structure and girder [6,7]. Rather than attempting to determine the frequency of all the sources of mechanical vibrations effecting the TBM, here the approach has been taken to determine and optimise the natural frequency of the Modules, and to avoid inducing large oscillations at critical frequencies.

The TBM designs proposed here (Section 2) utilise a 'hard-mount' passive vibration isolation system [8], similar to the one proposed for the prealignment bases of the main beam quadrupoles (MBQs) [9,10], and unlike the pre-isolation of the CLIC final focusing magnets which use 'soft-mount' isolation systems [11]. Such systems aim to maximise the ability of the supports to withstand external disturbances by increasing the stiffness of the base, and increasing the natural frequency of the system to greater than the frequencies of most concern [11].

* Corresponding author.
E-mail address: matthew.john.capstick@cern.ch (M. Capstick).

https://doi.org/10.1016/j.nima.2022.166834
Received 20 February 2022; Received in revised form 21 April 2022; Accepted 29 April 2022
Available online 10 May 2022

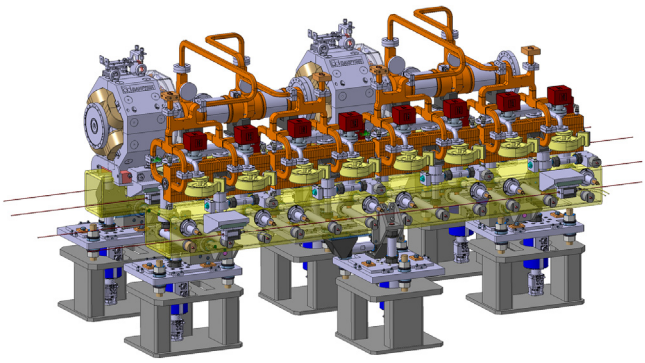

Fig. 1. A CLIC Two Beam Module (TBM).

The CLIC beam trajectory feedback system is good at suppressing frequencies below 1 Hz but amplifies frequencies the range 4–25 Hz, and those immediately above and below the operational frequency of CLIC, therefore mechanical vibrations in this range should be avoided [11]. Vibrations exactly at the 50 Hz repetition frequency (or multiples thereof) will appear as a static imperfection to the beam, and must fall within the prealignment tolerances. Finally, it is desirable to avoid low harmonic frequencies as sources of mechanical vibration typically ramp-up from 0 Hz to a certain steady state frequency, and inducing large displacements during this process could affect the pre-alignment. For these reasons, the goal of this optimisation process will be to increase the fundamental frequency of the system to significantly greater than the 50 Hz operating frequency [12].

2. Module design

The CLIC Two Beam Module design employs two separate structural members, or girders, onto which the drive beam and main beam components will be mounted. Components are pre-aligned relative to each other using a Coordinate Measuring Machine (CMM) before the modules are installed within the CLIC tunnel. This technique has been developed and demonstrated as part of the PACMAN project [13–15]. To accommodate manufacturing errors in the structures and girders the pre-alignment system requires a resolution of <1 μm over a range of 3 mm. Once installed within the tunnel the structural support members will be actively positioned relative to the machine reference network. This system requires a resolution of <1 μm over a range of 6 mm. Within the design proposed here, a standard rectangular-section steel beam is used to optimise the stiffness of the girder while also reducing the overall cost of each module. A schematic of this system is shown in Fig. 2. A klystron powered CLIC module would use the same design for the main beam support system in isolation.

2.1. Flexures

Within the previous module designs, the pre-alignment of the beam-line components has been achieved using a kinematic support based around six mechanical flexures [16]. By utilising flexures designed to be mechanically stiff in a single axis, but relatively flexible in all others, it is possible to construct a support structure that precisely and independently constrains each degree of freedom.

The stiffness of the flexures is determined by their geometry, particularly the diameter of the flexure at its narrowest point, and the radius of the curvature on either side of this point. A flexure with a high off-axis stiffness will accommodate a low adjustment range and vice versa. Examples are shown in Fig. 3.

Table 1
The jitter tolerances of the CLIC Super Accelerating Structures (SAS) [1].

	SAS (Main Beam)
Vertical tolerance	1.4 μm
Lateral tolerance	8 μm
Longitudinal tolerance	8 μm
Pitch tolerance	1.1 μrad
Yaw tolerance	6 μrad
Roll tolerance	5 mrad[a]

[a]The roll position tolerance of the structure is considerably lower than the other tolerances due to the axial symmetry of the structure cells; however, a tolerance of 5 mrad is still required to allow the mechanical integration of the structures.

2.2. Cam movers

Alternative girder support systems using either five or six eccentric cams have also been considered. Both are shown in Fig. 4. Achieving prealignment and active positioning of components using both these schemes has previously been demonstrated [17,18]. Both will be considered for their use within the CLIC TBM due to their high stiffness [19]. It was demonstrated that the harmonic frequencies of such systems can be increased by increasing the normal force on the cams; however, this increases the influence of static friction, and consequentially lowers the achievable movement resolution [20,21]. Due to the cost and complexity of these systems, cam movers have only been considered for the active girder alignment system, and not the passive structure prealignment system.

2.3. Universal joints

A final alternative is also considered here. This system relies upon the same kinematics as the flexure system; however, ‘universal joints’ are used instead of flexures. Designed for HL-LHC, these joints are rigid in one axis but accommodate motion in all other degrees of freedom [22]. This is achieved using two sintered bronze self-lubricating spherical bearings mounted in series. The bearings are installed between the central core and a high strength steel (34CrNiMo6) cap. See Fig. 5.

2.4. Waveguide network

Several additional components are mounted to the SAS, including; RF loads, vacuum pumps, and the power distribution waveguides. Collectively these components (shown in Fig. 6(a)) will be referred to as the waveguide network. These additional components increase both the total mass and the height of the centre-of-mass (COM). Since both of these factors negatively effect the natural frequency of the system, they have been investigated here. Initial studies suggest that a moderate reduction in the size of the waveguide network around the structures is possible, but may require significant modifications to the design of many components. An investigation will be carried out here to determine whether these reductions are necessary to meet the CLIC stability requirements.

3. Joint axial stiffness

To determine the suitability of the ‘universal joints’ (shown in Fig. 5) for use within the CLIC TBM support system, the axial stiffness of these joints must be understood, quantified, and optimised. It would be very computationally intensive to accurately model each joint in three-dimensions within a larger modal analysis. Instead, the axial stiffness of the joints will be determined separately using a 2D-Axisymmetric analysis.

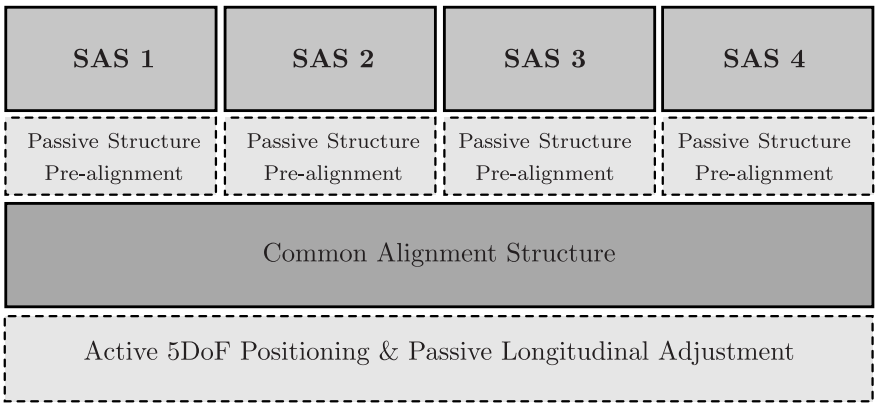

Fig. 2. A schematic of the CLIC TBM alignment system.

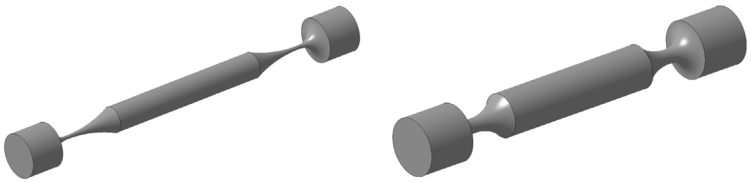

(a) A low stiffness, high adjustment range flexure.

(b) A high stiffness, low adjustment range flexure.

Fig. 3. Two mechanical flexures designed for different on-axis and off-axis stiffnesses.

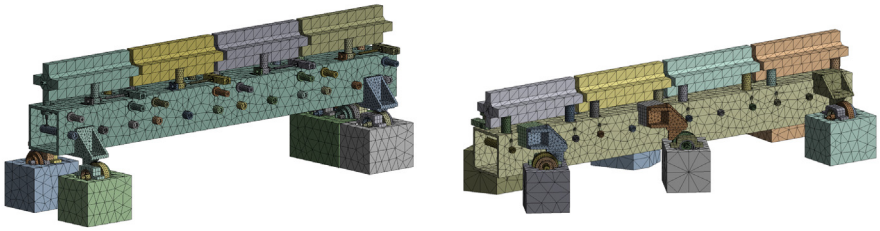

(a) 5 axis cam system.

(b) 6 axis cams system.

Fig. 4. An image of the two cam system configurations.

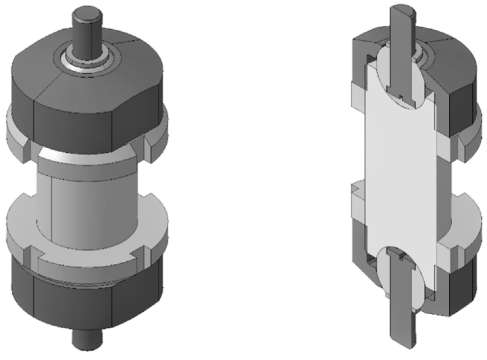

(a) (b)

Fig. 5. A universal joint shown in isometric (a) and cross-section (b).

3.1. 2D-axisymmetric analysis

Due to the symmetric design of the joints, the analysis was performed using 2D-Axisymmetric geometry. This greatly reduces the computation time, and allows a fine mesh to accurately model the contact (Fig. 7). The contact area between the spherical bearing and the socket components is critically important when determining the axial stiffness. Idealised geometry would imply a line contact between the two components, and therefore a point contact in the 2D analysis; however, experience with joint prototypes suggests that this is incorrect, and that close to 50% of the available bearing surface area is in contact. Both situations are considered here.

A preload must be applied to the cap during the assembly. Physically this is achieved by tightening the cap onto the threaded core component. Within the analysis this is achieved in an initial load-step. After this preload, a bonded contact is activated between the cap and the core. This deforms the mesh around the contact regions as expected, and allows the remainder of the analysis to be carried out independently. The deformation of the assembly after the preload step is shown in Fig. 7(b). Note the large displacement of the cap relative to the core due to the sliding contact.

The force–displacement curve produced for a joint with 14 mm diameter bearings modelled with line contact is shown in Fig. 8(a). In

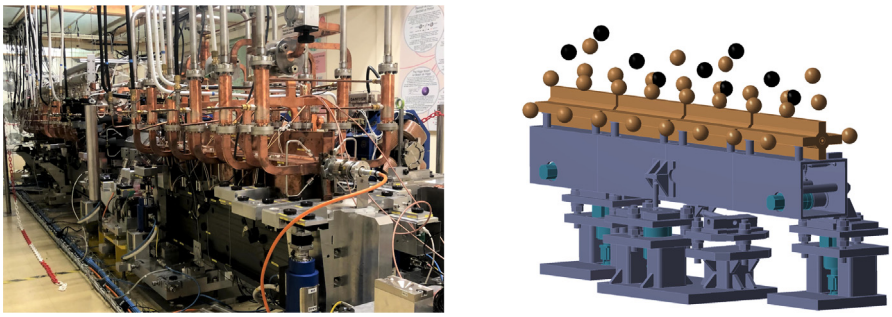

(a) A CLIC module prototype including all waveguide-network components.

(b) A CLIC module model including waveguide-network point masses.

Fig. 6. An image of a prototype CLIC module assembly (a) and a similar module modelled within FEA (b).

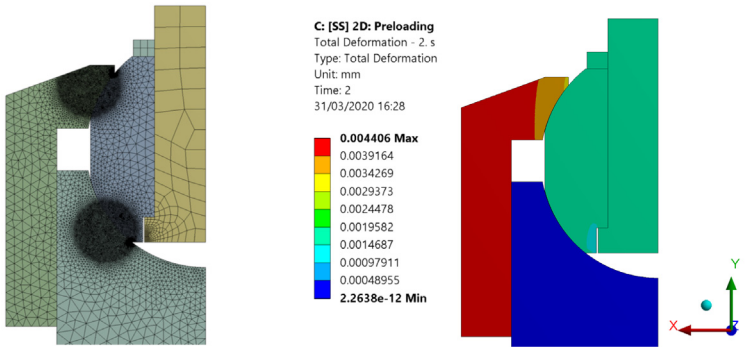

(a) The mesh used for analysis.

(b) The deformation of the spherical bearing under preload.

Fig. 7. Joint analysis mesh undeformed (a) and after preload (b).

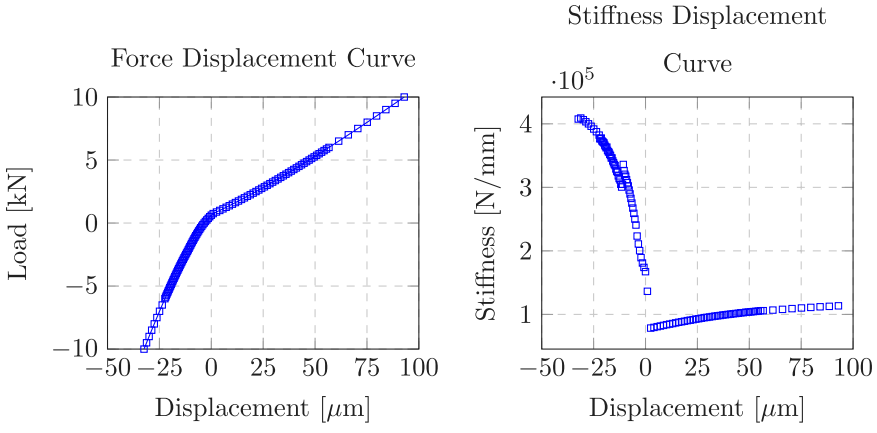

(a) Load-displacement results

(b) Stiffness-displacement results

Fig. 8. The calculated response of a 14 mm diameter bearing assembly under load, assumed to have an initial line contact.

Fig. 8(b) the stiffness is plotted directly against displacement. In both charts there is a noticeable difference stiffness between compression and tension. The larger compressive stiffness increases with negative load, and the lower tensile stiffness increases with positive load. Additionally there is a middle ground where, due to the preload, there is contact on both the upper and lower surfaces of the bearing. This becomes more or less significant depending on the magnitude of the applied preload, and if a large contact area is assumed.

The contact area, amount of preload applied, and the diameter of bearing all effect joint stiffness, with the bearing diameter being the most significant factor. Fig. 9 shows the relationship between bearing diameter and joint stiffness.

3.2. Joint design optimisation

Based on this analysis, it is clear that the design of the joints can be optimised for use within a CLIC module. The contact area percentage will be assumed to be 50%, matching the physical inspection of the joint prototype, and the preload will be fixed at 250 N as higher preload is likely to limit the travel of the joint without significantly increasing

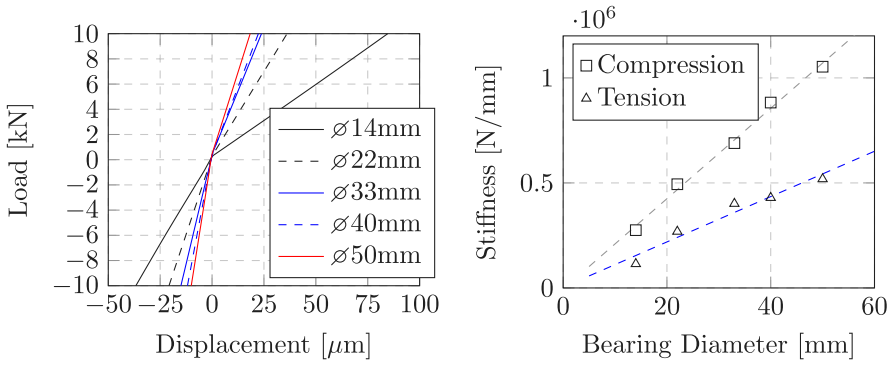

(a) The force-displacement curves for optimised joints with various bearing diameters.

(b) Joint bearing diameter compared to compressive and tensile joint stiffness.

Fig. 9. The results of analysis of the optimised joint analyses.

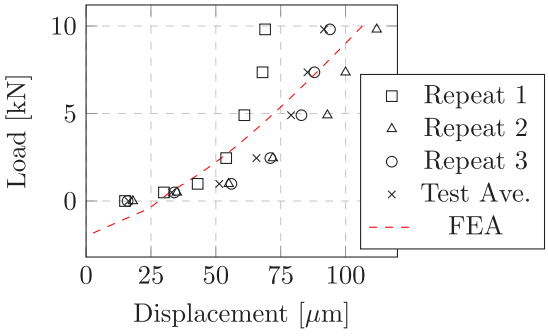

Fig. 10. The results of compressive testing of a ⌀22 mm prototype universal joint.

the joint stiffness. The diameter of the joint can be considered a variable within the modal and harmonic analyses which requires optimisation. The results of this will be covered in Section 4.2.

3.3. Joint prototype testing

Prototype universal joints of various diameters have been manufactured and tested by the Geodetic Metrology group at CERN. The results of a compressive test for a ⌀22 mm universal joint is given in Fig. 10. Also plotted is the force–displacement curve produced when a joint with the same geometry was recreated in FEA. A noticeable amount of backlash occurred during the prototype testing, to account for this the results of the simulation have been offset by 25 µm for easy comparison. The FEA shows a good agreement with the results of the physical testing, suggesting that the model is accurate and the behaviour of the sintered bronze bearings is well represented within FEA.

A prototype joint was also installed within an individual structure alignment platform and the kinematics of the system were tested. Within these tests, the structure was able to be positioned to within the CLIC alignment tolerances, as measured by a contact probe, suggesting that the kinematics of the alignment system are not limited due to the inclusion of the joint. Here the sintered bronze bearings performed as expected without a significant static friction effect at the small amplitudes of concern.

3.4. Non-linear joint approximations

The force–displacement curves, such as the one shown in Fig. 8(a), can be extracted from the 2D analysis and applied to a single element within a larger modal or harmonic analyses. Practically this is achieved within the Finite Element Analysis software ANSYS by inserting a COMBIN39 non-linear element using an ADPL command [23]. When used in series with a four-degree of freedom 'slot' joint or constraint equation and a linear spring to replicate the behaviour of the central core, the kinematics and stiffness of a universal joint can be replicated using a fraction of the computational power required for a full 3D analysis. A schematic of this arrangement is shown in Fig. 11.

4. Modal analysis

The FEA software ANSYS Mechanical 2019 R1 [24] was used to determine the modal frequencies of the main beam assembly. FEA can be used to determine the resonant frequencies of a system by establishing the stiffness matrix of the system and extracting the Eigenfrequencies. Using this method, the effect that the flexure/joint design, supported mass, and the base support design has on the modal frequencies will be found.

4.1. Flexure support systems

As discussed in Section 2.1, an important consideration in the design of the flexures is their stiffness. The axial stiffness influences the harmonic frequencies of any support system, and the off-axis stiffness influences the adjustment range of the support system. As the range is a more useful value for comparison, the analyses here will compare the fundamental frequency to adjustment range. The adjustment range for each system is determined using a static analysis of the highest stress configuration, where the peak stress is kept below the yield stress of the material used (1050 MPa for 34CrNiMo6 grade steel [25]).

Modal analysis was performed for two systems; one relying on flexures for the support of the girder, the other relying on a six-axis cam mover system. For each of these systems, the SAS are supported on a flexure-based six-axis prealignment platform. Several different SAS alignment flexures were considered, each providing a different prealignment adjustment range.

Modal analysis of the cam mover systems required modelling the bearings using stiffness matrices calculated using an established method from existing literature [17,19,26,27].

A five-axis cam mover system was also considered, however, this resulted in a significantly lower fundamental frequency than the six degree-of-freedom (DOF) system, largely due to the primary harmonic mode. This mode induced a lateral oscillation (or swaying) across the beam axis. The axes of the eccentric cams within the five-DOF system are parallel to the beam axis, therefore the primary mode can result in frictional sliding across the cams (Fig. 4(a)). In a six-DoF system, the eccentric cams axes are non-parallel and this sliding is not possible

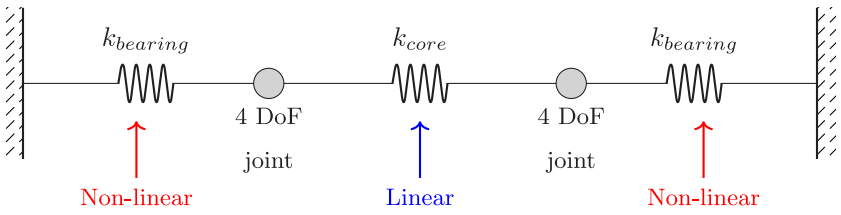

Fig. 11. The spring model of a universal joint.

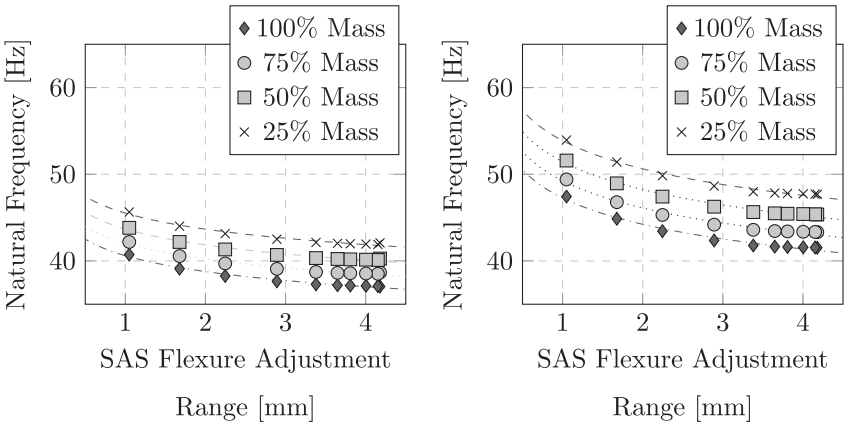

(a) Flexure supported girder. (b) Cam mover supported girder.

Fig. 12. The natural frequency [Hz] of the flexure supported Main Beam girder compared to the adjustment range of the SAS flexures [mm] for the three waveguide system masses considered.

(Fig. 4(b)). For this reason, the five-axis system will no longer be considered here.

Finally, the analyses were repeated with an assumed reduction in the mass supported by the waveguide system. The waveguide network was approximated using point masses coupled to SAS geometry, as shown in Fig. 6. These point mass values were then scaled to 100%, 75%, 50%, and 25% of their original values. The results are is given in Fig. 12.

For both support base configurations, the reduction of the size of the waveguide network and the flexure adjustment range increases the natural frequency of the system. For the flexure-supported girder the maximum achieved natural frequency is 45.6 Hz, which is close to, but not greater than 50 Hz as originally stated in the specification. In the case of the cam-mover-supported system the maximum achieved natural frequency is 53.9 Hz, which is not significantly greater than the 50 Hz operational frequency of CLIC.

Extrapolating the trends shown in Fig. 12 indicates that a solution could be found using a cam-mover system, however, this will not be considered any further for several reasons. Limiting the SAS adjustment system to a range of <1 mm is unacceptable due to the manufacturing tolerances on the outside surfaces of the SAS, and the required reduction in mass of the waveguide network would pose a significant engineering challenge. Finally, an alternative solution has been found which does not have these limitations and will be discussed in Section 4.2.

4.2. Universal joint support systems

As discussed in Section 3.2, the joint bearing diameter has a significant impact on the axial stiffness of the joint. Changing the joint stiffness will affect the harmonic response of the whole module therefore multiple analyses have been performed with varying joint diameters to investigate this effect. The results of these analyses are shown in Fig. 13. The frequency of the fundamental mode of the module increases with the diameter of the bearings within the joint. The

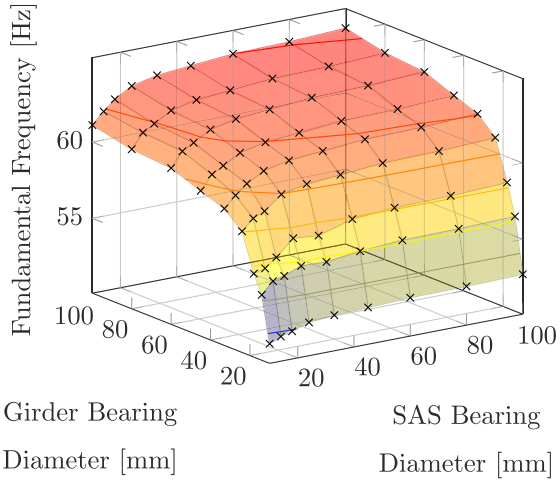

Fig. 13. The fundamental frequency of the joint-supported main beam assembly for various joint designs.

diameter of the bearings used for the support of the girder have a more significant effect on the fundamental frequency than the diameter of the SAS support bearings. The largest diameter joints considered had a diameter of 100 mm and achieved a fundamental frequency of close to 65 Hz; however, increasing the diameter produced diminishing returns at larger diameters. Additionally, the difficulty of integrating a joint of this size within the SAS pre-alignment systems would likely prevent its use.

A module which uses ⌀35 mm bearings for the girder supporting joints and ⌀22 mm bearings for the SAS supporting joints achieved a fundamental frequency of 60 Hz. This has been chosen as a compromise between higher-stiffness designs and the limited practical size of the

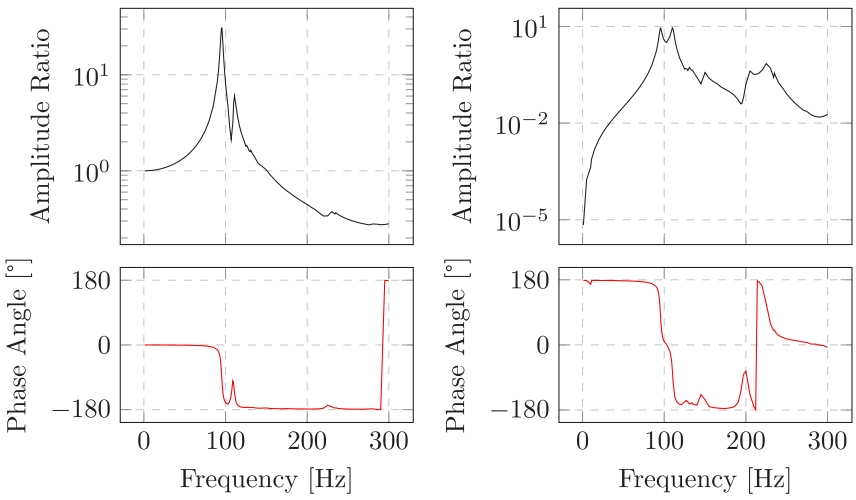

(a) Z Axis SAS frequency response. (b) Y axis SAS frequency response.

Fig. 14. The frequency response of the module due to in-phase base excitation in the z axis and measured at the beam axis.

joints. A TBM design based on these joints has been created and is shown in Fig. 1.

Only the fundamental mode was used for this optimisation; however, the fundamental mode shape primarily involves the module swaying laterally across the beam axis, so the vertical jitter caused by this vibration is significantly less than the lateral jitter. As stated in Section 1, the vertical jitter tolerance is significantly tighter than the lateral jitter tolerance, so the higher order modes should also be considered. For this module design, the harmonic mode which produces the greatest vertical displacement occurs at 103 Hz.

4.3. Modal analysis conclusion

The analysis detailed in Section 4.1 demonstrated that a CLIC module support system entirely based around flexures is unlikely to reach the stability requirements without critically limiting the adjustment range of the system and the mass of the waveguide components. Replacing the girder-supporting flexures with a six-axis cam mover system was shown to achieve a significant increase in stiffness, and so increased the natural frequency of the system significantly. Despite this increase, in order to reach the stability requirement of the CLIC module the range of SAS supporting flexures would still need to be reduced to <1 mm and the mass of the waveguide system would be limited. In Section 4.2 a system which utilises the same kinematics as the flexure adjustment system, but relies upon 'universal joints' has been shown to provide the stiffness required without limiting the adjustment range of the systems. The stiffness of each joint is highly dependent on the diameter of the bearings used. Using 22 mm diameter bearings for the support of the SAS and 35 mm bearings for the support of the girder provides the stiffness required without restricting the integration due to the size of the joints. At very large joint diameters, the fundamental frequency of the system no longer proportionally increases, this is because other components in the system (for example, the linear actuators [28]) have a finite stiffness and therefore limit the maximum fundamental frequency which can be reached.

5. Ground noise vibration

The analysis detailed in Section 4 determined the TBM harmonic frequencies. This is useful as a method to identify and mitigate the impact which unknown sources of vibration can have on the functionality of the CLIC main LINAC. In cases where a source of vibration is well known, further analysis can be carried out to quantify the resulting vibrations of the accelerating structures. These displacements can then be compared to the CLIC operational requirements.

5.1. Harmonic analysis

The model detailed in Section 4.3 was carried forward and a harmonic analysis was performed. Within this analysis a harmonic displacement with a nominal amplitude was applied the base of the module, and a sweep across the frequency range was performed. A damping ratio of 3% was assumed, a generally accepted value for continuous steel structures [29]. Initially, the excitation of all three bases of the main beam girder were assumed to be in-phase with each other. This is consistent with the coherence of the ground vibrations measured within the LHC when considered over the length 2 m length of a single module [30] and below a frequency of around 100 Hz [3]. The separate response of each acceleration structure was determined, as was an average of the four SAS to represent the overall module response. For simplicity the module average response will be given here.

The plots in Fig. 14 show the frequency response function of the joint-supported module, when exposed to an in-phase vertical base excitation. Fig. 14(a) shows the vertical response of the module. Fig. 14(b) shows the lateral response of the same module.

The plots in Fig. 15 show the frequency response function of the joint-supported module, when exposed to an out-of-phase vertical base excitation. Fig. 15(a) shows the vertical response of the module measured at the beam axis. Fig. 15(b) shows the lateral response of the module.

The harmonic response of the module shows an amplification of the vertical base vibrations up to 150 Hz, with a noticeable peak around 100 Hz. This peak aligns with the harmonic mode which produces the greatest amount of vertical jitter, as discussed in Section 4.3. This response is typical of a hard-mount passive vibration isolation system such as this one.

5.2. Ground noise analysis

CLIC is proposed to be constructed at CERN, across the French/Swiss border close to Geneva. The typical ground noise vibrations in this region are very well categorised [30]. Fig. 16 shows the Power Spectral Density of the vertical displacement of the ground measured at two points within the Large Hadron Collider (LHC) tunnel. Within these data a peak between 0.1 Hz and 1 Hz can be seen; this is the microseismic peak attributable to wave motion within the oceans [31]. Above 1 Hz the ground motion is affected by local technical noise, such as nearby machinery or services, which leads to noticeable differences between the two LHC locations.

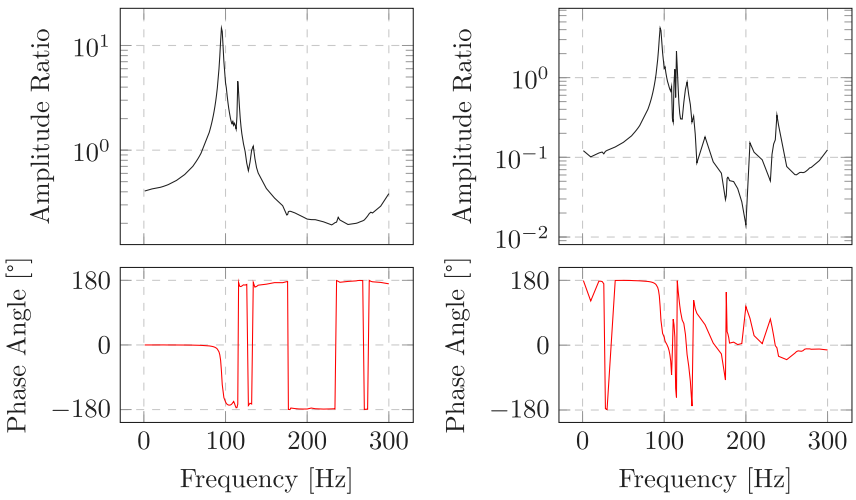

(a) Z Axis SAS frequency response. (b) Y axis SAS frequency response.

Fig. 15. The frequency response of the module due to out-of-phase base excitation in the z axis and measured at the beam axis.

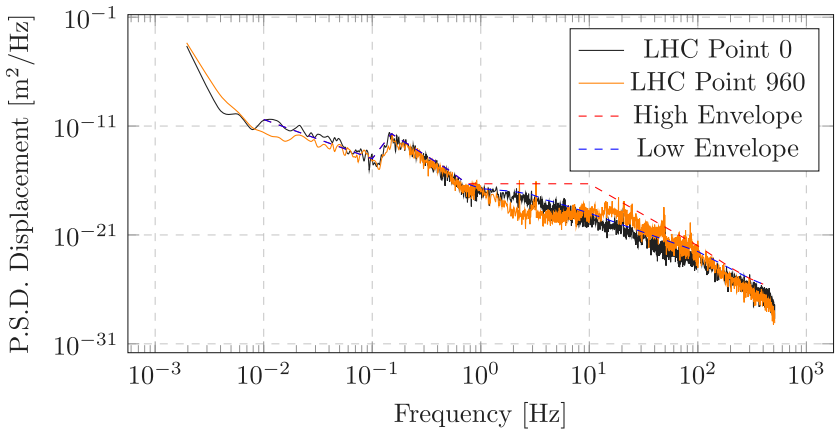

Fig. 16. Power Spectral Density of ground displacement measured at two points within the LHC.

Further analyses were carried in order to determine the P.S.D displacement response of the module and the statistical misalignments of the structures due to ground noise. Within ANSYS this is achieved using a random noise analysis, where the excitation is the ground noise data shown in Fig. 16. For ease of analysis, the maximum envelope curve shown in Fig. 16 will be used as a conservative simplification of the ground noise data. Fig. 17 shows the same envelope curve of the input data as well as the x, y, and z response displacement P.S.D. of the module due to this input excitation. The fundamental frequency as well as the higher order harmonic frequencies can easily be identified due to the peaks in displacement above the input. As expected, the fundamental mode produces a much greater response in the longitudinal (X) and lateral (Y) axes than the vertical axis (Z). A noticeable dampening of the displacement can also be seen at higher frequencies >200 Hz.

These results agree with the harmonic analysis detailed in Section 5.1. The transfer functions shown in Fig. 14 and Fig. 15 indicated that the module will not experience large displacements above ground noise due to ground vibrations <50 Hz. This can also be determined from Fig. 17 as there is no distinguishable difference between the input and output P.S.D at frequencies significantly below the natural frequency.

As the displacement of the ground at any given point and time cannot be accurately predicted, the displacement of each accelerating structure must be defined statistically. Assuming that the displacement due to ground noise of each of the individual accelerating structures along the LINAC follows a normal distribution, the standard deviation can be used to evaluate the impact the ground noise will have on the overall alignment of the LINAC. An important consideration is the frequency range of the ground noise. As can be seen in Fig. 16, the ground motion approximately follows a steep function of frequency which falls off as $\frac{1}{f^4}$, and including all the data given produces very large numerical displacements occurring due to the low frequency noise, which is not of concern here. Two analyses were carried out; one used 1 Hz as the lower limit as vibrations below this frequency are well suppressed by the CLIC beam trajectory feedback system [11], the other used 0.1 Hz as the lower limit as the ground noise is coherent over lengths around 1 km between 0.1 Hz and 1 Hz [3]. For both these cases, the 1σ displacements for each structure have been calculated and are included in Table 2.

6. Conclusions

A module design has been presented and optimised using Finite Element Analysis with a fundamental frequency of 60 Hz, significantly greater than the 50 Hz operational frequency of CLIC. Capacity for further optimisation to increase the fundamental frequency to 64 Hz has also been shown, but is currently not considered necessary. The historical ground noise data from the LHC at CERN was used to statistically quantify the magnitude of the unavoidable induced misalignments of

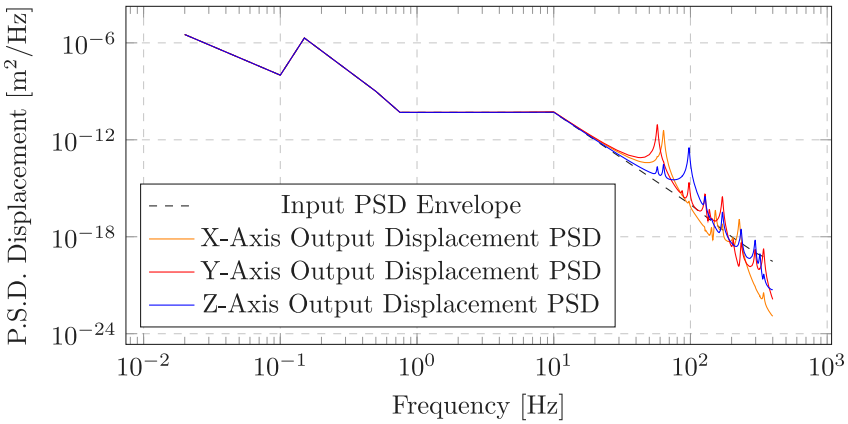

Fig. 17. Power Spectral Density of module response due to known ground noise.

Table 2
The one-standard-deviation displacement of each accelerating structure on a module in each axis relative to the ground motion, and for three difference frequency ranges.

1σ Displacement [μm]				
		Frequency Range		
Structure	Axis	0.08 Hz+	0.1 Hz+	1 Hz+
SAS 1	X	0.3633	0.0149	0.0028
	Y	1.0773	0.0278	0.0034
	Z	0.6194	0.0399	0.0011
SAS 2	X	0.3594	0.0158	0.0028
	Y	1.4495	0.0269	0.0034
	Z	0.5640	0.0432	0.0010
SAS 3	X	0.4274	0.0148	0.0028
	Y	1.6129	0.0282	0.0035
	Z	1.1728	0.0444	0.0010
SAS 4	X	0.6316	0.0140	0.0028
	Y	1.3604	0.0290	0.0032
	Z	1.2654	0.0413	0.0010
Average	X	0.4451	0.0149	0.0028
	Y	1.3750	0.0280	0.0034
	Z	0.9054	0.0422	0.0010

the SAS due to the local ground noise. From this analysis the one-sigma vertical misalignment due to ground noise above 0.1 Hz was less than 0.044 μm for each SAS, and less than 0.042 μm averaged across all four SAS.

The scope of this work so far has been limited to Finite Element Analysis, which has, where possible, been validated using data from physical testing. Future work on the CLIC module should include the manufacture and testing of a full scale prototype in order to fully validate the analysis discussed here.

Declaration of competing interest

The authors declare that they have no known competing financial interests or personal relationships that could have appeared to influence the work reported in this paper.

Data availability

The data, computational models, and test results used to support this study can be made available upon reasonable request from the lead author.

Acknowledgements

The authors would like to thank Alex Vamvakas and Henri Berg for their preliminary studies towards the present work. We also thank Kurt Artoos and Juha Kemppinen for their valuable advice on the analysis performed, and for providing the LHC ground noise data used. We would like to thank Mateusz Sosin, Hélène Mainaud-Durand, and Callum Maclean for their work on the design, development, and testing of the Universal Joints. Finally, thanks to Andrea Latina and Daniel Schulte for their assistance and advice regarding the CLIC main LINAC component transient position requirements.

References

[1] M. Aicheler, P. Burrows, M. Draper, T. Garvey, P. Lebrun, K. Peach, N. Phinney, H. Schmickler, D. Schulte, N. Toge, A multi-TeV linear collider based on CLIC technology: CLIC conceptual design report, in: CERN Yellow Reports: Monographs, CERN, Geneva, 2012, http://dx.doi.org/10.5170/CERN-2012-007, URL https://cds.cern.ch/record/1500095.

[2] P. Lebrun, L. Linssen, D. Schulte, E. Sicking, S. Stapnes, M. Thomson, P. Burrows, M. Boland, U. Felzmann, P. Giansiracusa, T. Lucas, R. Rassool, C. Balázs, T. Charles, K. Afanaciev, I. Emeliantchik, A. Ignatenko, V. Makarenko, N. Shumeiko, M. Woodley, Updated Baseline for a Staged Compact Linear Collider, 2016, http://dx.doi.org/10.5170/CERN-2016-004.

[3] M. Aicheler, P.N. Burrows, N. Catalan, R. Corsini, M. Draper, J. Osborne, D. Schulte, S. Stapnes, M.J. Stuart, The compact linear collider (CLIC) - project implementation plan, in: M. Aicheler (Ed.), in: CERN Yellow Reports: Monographs, 2019, http://dx.doi.org/10.23731/CYRM-2018-004.

[4] T.O. Raubenheimer, Estimates of emittance dilution and stability in high-energy linear accelerators, Phys. Rev. Spec. Top. Accelerators Beams 3 (12) (2000) 121002, http://dx.doi.org/10.1103/PhysRevSTAB.3.121002, URL https://link.aps.org/doi/10.1103/PhysRevSTAB.3.121002.

[5] P. Cabral, M. Nonis, Cooling and ventilation studies for the CLIC, Tech. Rep. CERN-ACC-2020-0025. CLIC-Note-1164, CERN, Geneva, 2019, URL http://cds.cern.ch/record/2732035.

[6] F. Le Pimpec, S. Adiga, F. Asiri, G. Bowden, E. Doyle, B. McKee, A. Seryi, S. Redaelli, Vibrational stability of NLC linac accelerating structure, 2002, URL https://accelconf.web.cern.ch/e02/PAPERS/MOPRI119.pdf.

[7] L. Zhang, L. Farvacque, M. Lesourd, E. Plouviez, Electron beam stabilization experiences at the ESRF, 2002, URL https://www.researchgate.net/publication/229034574_ELECTRON_BEAM_STABILIZATION_EXPERIENCES_AT_THE_ESRF.

[8] L. Lacny, M. Kozień, D. Ziemiański, Selected overview of the impact of ground motion on the vibrations of particle accelerators, AIP Conf. Proc. 2239 (1) (2020) 020025, http://dx.doi.org/10.1063/5.0008950, URL https://aip.scitation.org/doi/abs/10.1063/5.0008950.

[9] S. Janssens, C. Collette, K. Artoos, P. Fernandez Carmona, C. Hauviller, A Sensitiviy Analysis for the Stabilization of the CLIC Main Beam Quadrupoles, Tech. Rep., 2010, URL https://cds.cern.ch/record/1297980/files/EuCARD-CON-2010-025.pdf.

[10] C. Collette, K. Artoos, A. Kuzmin, S. Janssens, M. Sylte, M. Guinchard, C. Hauviller, Active quadrupole stabilization for future linear particle colliders, Nucl. Instrum. Methods Phys. Res. A 621 (2010) 71–78, http://dx.doi.org/10.1016/j.nima.2010.05.020.

[11] C. Gohil, Dynamic Imperfections in the Compact Linear Collider (Ph.D. thesis), 2020, URL http://cds.cern.ch/record/2724824/files/CERN-THESIS-2020-074.pdf.

[12] H. Berg, Thermal and Modal Simulations for the CLIC Module, Tech. Rep., Helsinki Institute of Physics, 2020.

[13] P. Arpaia, D. Caiazza, N.C. Lasheras, N.G. Munoz, S. Kamugasa, H.M. Durand, M. Modena, S. Sanfilippo, C. Sanz, G. Severino, S. Zorzetti, PACMAN: PArticle accelerator components metrology and alignment to the nanometre scale, 2016, URL https://pacman.web.cern.ch/pacman/.

[14] H. Mainaud Durand, K. Artoos, B. Marco, D. Caiazza, N. Catalán Lasheras, A. Cherif, I. Doytchinov, J.-F. Fuchs, A. Gaddi, G.M. Natalia, J.-C. Gayde, S. Kamugasa, M. Modena, P. Novotny, S. Russenschuck, C. Sanz, G. Severino, D. Tshilumba, V. Vlachakis, M. Wendt, S. Zorzetti, PACMAN Project: A new solution for the high-accuracy alignment of accelerator components, 2016, MOOCB01. 4 p, http://dx.doi.org/10.18429/JACoW-IPAC2016-MOOCB01. URL http://cds.cern.ch/record/2207305.

[15] H. Mainaud Durand, K. Artoos, B. Marco, D. Caiazza, N. Catalan Lasheras, A. Cherif, I.P. Doytchinov, J.-F. Fuchs, A. Gaddi, G.M. Natalia, J.-C. Gayde, K.S. William, M. Modena, P. Novotny, C. Sanz, G. Severino, S. Russenschuck, D. Tshilumba, V. Vlachakis, M. Wendt, S. Zorzetti, Fiducialisation and initial alignment of CLIC component with micrometric accuracy, 2016, URL https://cds.cern.ch/record/2237694.

[16] N. Gazis, G. Riddone, H. Durand, D. Gudkov, A. Samoshkin, S. Simopoulos, E. Hinis, T. Alexopoulos, Study of the supporting system for the CLIC two-beam module, J. Eng. Sci. Technol. Rev. 4 (2011) 201–206, http://dx.doi.org/10.25103/jestr.042.14.

[17] J. Kemppinen, S. Griffet, R. Leuxe, H. Mainaud Durand, J. Sandomierski, M. Sosin, CLIC Main Beam Quadrupole Active Pre-Alignment Based on Cam Movers, Tech. Rep., 2012, URL https://cds.cern.ch/record/1519140.

[18] M.-H. Wu, W.-Y. Lai, T.-C. Tseng, M.-L. Chen, H.-S. Wang, H.-C. Ho, C.-J. Lin, H.-M. Luo, S.-Y. Perng, P.-L. Sung, C.-S. Lin, H.-C. Lin, J. Chen, Design and Experiment of the Auto-alignment Control System for TPS Storage Ring Girder, Vol. 234, 2013, pp. 357–364, http://dx.doi.org/10.1007/978-1-4614-6747-2{_}43.

[19] J. Kemppinen, H. Durand, A. Herty, Improving high precision cam mover's stiffness, J. Phys. Conf. Ser. 1350 (2019) 012137, http://dx.doi.org/10.1088/1742-6596/1350/1/012137.

[20] J. Kemppinen, Z. Kostka, H.M. Durand, Cam Mover Alignment System Positioning with Wire Position Sensor Feedback for CLIC, Tech. Rep., 2016, URL https://cds.cern.ch/record/2238912/files/CERN-ACC-2016-0339.pdf.

[21] J. Kemppinen, CLIC Main Beam Quadrupole Alignment Using Cam Movers, Tech. Rep., 2017, URL https://indico.cern.ch/event/684351/.

[22] M. Sosin, T. Blaszczyk, H.M. Durand, A. Herty, J. Jaros, G. Switzerland, Design and study of a 6 degree-of-freedom universal adjustment platform for HL-LHC components, 2019, http://dx.doi.org/10.18429/JACoW-IPAC2019-THPGW058.

[23] Ansys INC, Mechanical APDL 2021 R2, product documentation, chapter 7 element library, COMBIN39, 2021, URL https://ansyshelp.ansys.com/.

[24] Ansys, Ansys® mechanical, release 2019 R1, 2019, URL https://www.ansys.com/.

[25] MatWeb, 34CrNiMo6 356Q Steel, hardening, material properties, 2021, URL http://www.matweb.com/.

[26] T.A. Harris, M.N. Kotzalas, Advanced Concepts of Bearing Technology, fifth ed., CRC Press, 2006, http://dx.doi.org/10.1201/9781420006582.

[27] T.C. Lim, R. Singh, Vibration transmission through rolling element bearings, part I: Bearing stiffness formulation, J. Sound Vib. 139 (2) (1990) 179–199, http://dx.doi.org/10.1016/0022-460X(90)90882-Z.

[28] M. Sosin, Qualification of Linear Actuators from ZTS VVÚ KOŠICE, Tech. Rep., CERN, 2011, URL https://indico.cern.ch/event/112520/.

[29] F. Orban, Damping of materials and members in structures, J. Phys. Conf. Ser. 268 (2011) 012022, http://dx.doi.org/10.1088/1742-6596/268/1/012022.

[30] K. Artoos, O. Capatina, C. Collette, M. Guinchard, C. Hauviller, M. Sylte, B. Bolzon, A. Jeremie, Ground Vibration and Coherence Length Measurements for the CLIC Nano-Stabilization Studies, Tech. Rep., 2009, URL http://cds.cern.ch/record/1223610/files/th5rfp081.pdf.

[31] C. Collette, K. Artoos, M. Guinchard, C. Hauviller, Seismic response of linear accelerators, Phys. Rev. Spec. Top. Accelerators Beams 13 (2010) http://dx.doi.org/10.1103/PhysRevSTAB.13.072801.